Attractor–repeller collision and the heterodimensional dynamics FREE

Vladimir Chigarev ; Alexey Kazakov ; Arkady Pikovsky

Check for updates

View Online   Export Citation   CrossMark

Articles You May Be Interested In

Photoinduced currents in carbon nanotube/metal heterojunctions

Appl. Phys. Lett. (March 2006)

Mutual singularities of overlapping attractor and repeller

Chaos (August 2021)

Kantorovich–Rubinstein–Wasserstein distance between overlapping attractor and repeller

Chaos (July 2020)

Attractor–repeller collision and the heterodimensional dynamics

View Online   Export Citation   CrossMark

Vladimir Chigarev,[1,a] [ID] Alexey Kazakov,[1,b] [ID] and Arkady Pikovsky[2,c] [ID]

AFFILIATIONS

[1] National Research University Higher School of Economics, 25/12 Bolshaya Pecherskaya Ulitsa, 603155 Nizhny Novgorod, Russia
[2] Institute of Physics and Astronomy, University of Potsdam, Karl-Liebknecht-Str. 24/25, 14476 Potsdam-Golm, Germany

Note: This paper is part of the Focus Issue on Nonlinear dynamics, synchronization and networks: Dedicated to Juergen Kurths' 70th birthday.
[a] **Electronic mail:** vchigarev@hse.ru
[b] **Electronic mail:** kazakovdz@yandex.ru
[c] **Author to whom correspondence should be addressed:** pikovsky@uni-potsdam.de

ABSTRACT

We study the heterodimensional dynamics in a simple map on a three-dimensional torus. This map consists of a two-dimensional driving Anosov map and a one-dimensional driven Möbius map, and demonstrates the collision of a chaotic attractor with a chaotic repeller if parameters are varied. We explore this collision by following tangent bifurcations of the periodic orbits and establish a regime where periodic orbits with different numbers of unstable directions coexist in a chaotic set. For this situation, we construct a heterodimensional cycle connecting these periodic orbits. Furthermore, we discuss properties of the rotation number and of the nontrivial Lyapunov exponent at the collision and in the heterodimensional regime.

Published under an exclusive license by AIP Publishing. https://doi.org/10.1063/5.0144672

Hyperbolic dynamics is the most perfect form of chaos, with many nice mathematical and physical properties. However, in realistic systems, one often deals with not so perfect situations, where hyperbolicity is broken. One particular case of broken hyperbolicity is that of heterodimensional dynamics, where inside a chaotic set there are orbits with different numbers of unstable directions. In this paper, we present a particular mechanism of appearance of heterodimensional dynamics via a collision of a chaotic attractor and a chaotic repeller. We follow this transition by determining bifurcations of the periodic orbits embedded in the attractor and the repeller. We also demonstrate that heterodimensional dynamics has implications for the distribution of finite-time Lyapunov exponents.

I. INTRODUCTION

Hyperbolic chaotic sets are ideal objects with nice dynamical and statistical properties, however, they are quite rare in real applications. Hyperbolicity can be broken in many ways, and one particular case, that has attracted much attention recently, is that of *heterodimensional dynamics*, where different orbits inside a chaotic set have different numbers of positive Lyapunov exponents. In particular, periodic orbits embedded in chaos can have different numbers of stable and unstable directions. Remarkably, conclusions about the robustness of such a situation can be drawn just from the existence of so-called heterodimensional cycles[1]—trajectories, connecting periodic orbits with different dimensions of stable and unstable manifolds.

One of the first examples of hyperbolicity breaking associated with the existence of heterodimensional cycles was presented by Abraham and Smale.[2] The persistence of non-transversal intersections of invariant manifolds in such cycles was discovered and studied by Díaz and his collaborators.[3–5] The mathematical theory for maps with heterodimensional cycles of co-index one (where the difference between the dimensions of the unstable manifolds of the pair of saddle orbits connected by these cycles is one) was developed by Bonatti and Díaz,[1,6] where the authors proved the C^1-robustness of heterodimensional cycles. A more general higher smoothness version of this result has been recently obtained by Li and Turaev.[7] The results of Ref. 7 imply the existence of the heterodimensional dynamics caused by heterodimensional cycles in an appropriate

two-parameter family that unfolds an initial heterodimensional cycle.

In this paper, we explore a mechanism for the appearance of heterodimensional dynamics through a collision of a simple chaotic attractor with a simple chaotic repeller (both these objects are hyperbolic prior to the collision). Such a collision occurs naturally at the breakout of chaotic phase synchronization[8] (although in realistic situations one can hardly assume hyperbolicity). This collision is an extension of a simple saddle-node (tangent) bifurcation, responsible for the loss of synchrony of periodic driven oscillators, to the case of chaotic amplitude dynamics. We formulate the basic system as a chaotic hyperbolic subsystem (Anosov torus map), driving a circle map (Sec. II).

In the context of the chaotic phase synchronization applications,[8] the chaotic subsystem corresponds to the amplitude dynamics, and the circle map describes the driven phase dynamics. A stable regime of chaotic phase synchronization corresponds to the existence of a chaotic attractor on which the phase variations are bounded, roughly "in phase" with the driving. Since in the considered model the amplitude dynamics is invertible, there also exists a chaotic repeller (an attractor in the inverted time), roughly "in antiphase" with the driving. The dimensions of the stable and unstable manifolds of orbits on the attractor and on the repeller follow from one unstable and one stable directions of the Anosov map, and from the stability (instability) for the attractor (repeller) in the phase direction. As a parameter responsible for the "frequency mismatch" varies, the attractor and the repeller collide (Sec. III).

We show that this collision can be best traced through tangent bifurcations of periodic orbits embedded in chaos (Sec. IV). We argue that beyond the collision the attractor and the repeller overlap, and one chaotic set appears containing orbits with different dimensions of unstable manifolds. For two-dimensional reversible maps, the attractor-repeller collision was studied in Refs. 9–11 where it was also shown that after this a new type of chaotic dynamics—the so-called *mixed dynamics* appears. The mathematical theory of mixed dynamics was developed in Refs. 12–14; recent examples are given in Refs. 15–20.

Furthermore, we show in Sec. V that right beyond the attractor–repeller collision a heterodimensional cycle appears connecting a pair of saddle orbits from the former attractor and repeller. This implies, according to the Li and Turaev theorem,[7] that arbitrarily close to this cycle other heterodimensional cycles exist. Thus, one can say that the heterodimensional dynamics caused by the observed heterodimensional cycle is robust, i.e., it persists under variations of the parameter values.

II. MODEL

The basic model we study in this paper is a chaotically driven circle map. Because we want to have invertable equations, the driving chaotic map must be at least two-dimensional. We take a standard Anosov torus map (a.k.a. Arnold cat map) defined on a 2D-torus, which has nice properties: it is hyperbolic, and the stable and unstable manifolds can be easily found as straight lines on the torus. As a circle map we take a Möbius map,[21–24] which is readily invertible (for convenience, we summarize relevant properties of Möbius maps in the Appendix). Thus, the system under

investigation is an invertible map on 3D-torus $0 \leq t, s, x < 1$,

$$t_{n+1} = 2t_n + s_n \quad (\text{mod } 1), \tag{1a}$$

$$s_{n+1} = t_n + s_n \quad (\text{mod } 1), \tag{1b}$$

$$x_{n+1} = x_n + c + \mu \sin(2\pi t_n + \alpha)$$
$$- \frac{1}{\pi} \arctan\left(\frac{\varepsilon \sin 2\pi x_n}{1 + \varepsilon \cos 2\pi x_n}\right) \quad (\text{mod } 1). \tag{1c}$$

Here, Eqs. (1a)–(1b) describe the driving Anosov map; it has no free parameters. Equation (1c) is the driven Möbius map. The free Möbius map (i.e., with $\mu = 0$) has two parameters ε and c. Parameter ε determines how close is this map to a circle shift, which is realized for $\varepsilon = 0$. In the limit $\varepsilon \to 1$, almost the whole circle is mapped to a small neighborhood of one point on it. Parameter c is an additive one, it defines in a natural way the rotation number of the free Möbius map.

In some situations below, e.g., at calculations of the rotation number, it is convenient to lift map (1c) from the unit circle to the real line, in this case one just drops the operation (mod 1). We will denote the corresponding variable on the real line as $\tilde{x}_n$.

In the context of chaotic phase synchronization,[8] where a periodically driven chaotic attractor with a well-defined phase variable is studied, system (1) and the parameters have the following interpretations. The Anosov map (1a)–(1b) describes chaos of the amplitude variables of the attractor, while variable x in Eq. (1c) corresponds to the phase. Parameter μ describes "internal coupling" between the amplitude and the phase; it governs phase diffusion and is related to the level of coherence of free chaotic oscillations (larger values of μ correspond to a stronger phase diffusion, small values of μ mean almost regular phase rotations). Particularities of this internal coupling depend on the additional phase shift α. Terms c and ε describe the effect of the external periodic force on the chaotic attractor, their meaning is the same as in the context of a circle map reduction for forced periodic oscillations: c is roughly proportional to the frequency mismatch, while ε describes the strength of the forcing.

Below, we will describe attractors and repellers and their metamorphoses in dependence on the parameters. Parameter ε will be mainly fixed to $\varepsilon = 0.4$, due to the following reasons. Nontrivial dynamics of x disappears in the limit $\varepsilon \to 0$, where map (1c) is just the forced circle shift. On the other hand, in the limit $\varepsilon \to 1$ map, (1c) becomes singular. While one does not expect any qualitative dependence of the regimes described below in ε (see Fig. 4), mostly convenient for the numerical analysis and especially for visualization are "moderate" values of parameter ε.

III. PHENOMENOLOGY OF THE ATTRACTOR–REPELLER COLLISION

A. Attractor and repeller

We illustrate the chaotic attractor and the chaotic repeller in system (1) in Fig. 1. We depict long trajectories forward and backward in time, after discarding initial transients. These trajectories give impression on the invariant measures of the attractor and of the repeller. In the situation depicted in panel (a) these sets are separated, so that the attractor has its basin, and, in the forward
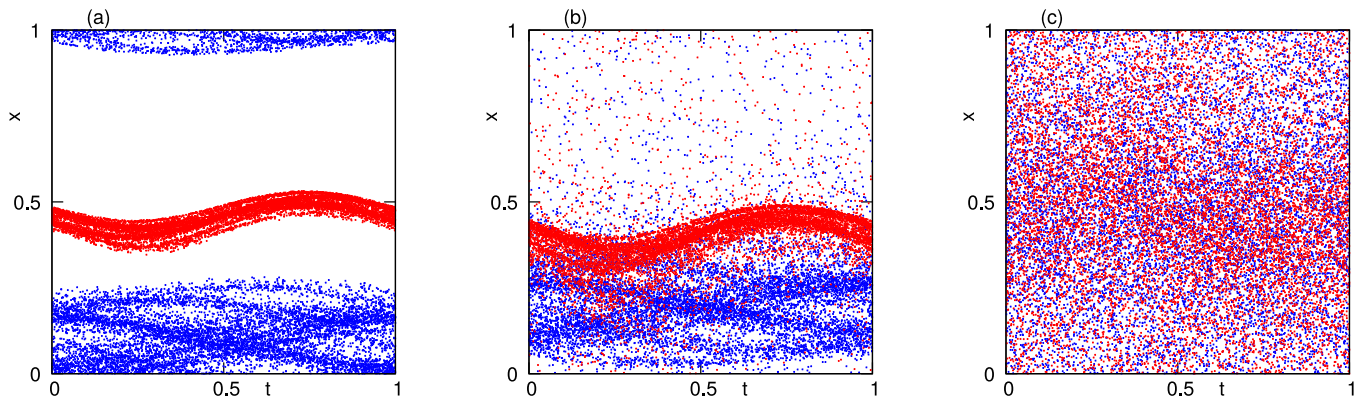
FIG. 1. Projections of the attractor (blue dots) and the repeller (red dots) for $\varepsilon = 0.4$, $\alpha = 0$, and $\mu = 0.1$. Panel (a): $c = 0.05$, the attractor and the repeller are separated; panel (b): $c = 0.1$, the attractor and the repeller overlap, but their measures are quite different; panel (c): $c = 0.4$, the measures of the overlapping attractor and repeller are quite similar.

time, the repeller serves as a chaotic saddle, close to which the long-lived transient dynamics occurs.[25] For the backward in time dynamics, these sets exchange their roles. Panels (b) and (c) show the case of overlapped attractor and repeller, where both sets are dense in the whole phase space (3D torus). However, the invariant measures of the attractor and the repeller are quite different in the case of panel (b), while for the case of panel (c) these measures nearly coincide. A transition from the separated attractor and repeller [Fig. 1(a)] to the overlapped chaotic set [Figs. 1(b) and 1(c)] is called *attractor–repeller collision.*[8]

B. Rotation number and the Lyapunov exponent

It is convenient to characterize the regimes in system (1) by means of the rotation number and the Lyapunov exponent, both calculated for the driven variable x.

The rotation number, both for the free and for the driven Möbius map, is defined as the mean velocity of rotations around the circle, using the lifted map,

$$\rho = \lim_{n \to \infty} \frac{\tilde{x}_n - \tilde{x}_0}{n} . \qquad (2)$$

It is clear that only the interval of values $-\frac{1}{2} \leq c < \frac{1}{2}$ is of interest, because $\rho(c \pm 1) = \rho(c) \pm 1$.

Another quantity we will calculate in numerical simulations with system (1) is the Lyapunov exponent (LE) in the x-direction. Indeed, because (1) is a skew system with driving variables (s, t), the three Lyapunov exponents are combined from the two Lyapunov exponents of the Anosov cat map (1a) and (1b) and of the Lyapunov exponent in the x direction from (1c). A direct calculation of the derivative of the r.h.s. of (1c)

$$\frac{dx_{n+1}}{dx_n} = \frac{1 - \varepsilon^2}{1 + 2\varepsilon \cos 2\pi x_n + \varepsilon^2}$$

yields the expression $\lambda = \left\langle \log \frac{dx_{n+1}}{dx_n} \right\rangle = \left\langle \log \frac{1-\varepsilon^2}{1+2\varepsilon \cos 2\pi x + \varepsilon^2} \right\rangle$. Here, the average should be taken according to the invariant measure on the

attractor; due to ergodicity it can be practically calculated as the time average.

We illustrate application of the rotation number and of the nontrivial Lyapunov exponent to the characterization of the attractor–repeller collision in Fig. 2. It shows profiles of the quantities ρ and λ in dependence on parameter c for fixed other parameters of the system. Both quantities are calculated in forward time (i.e., they
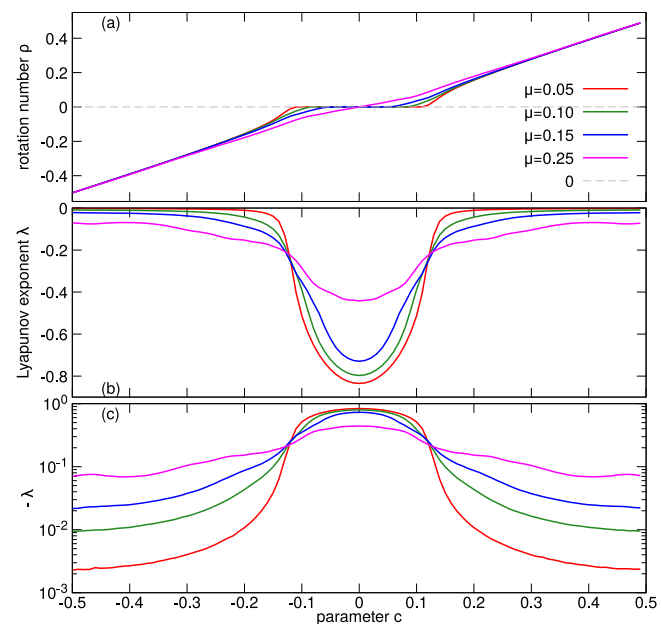

FIG. 2. Dependence of the rotation number [panel (a)] and the Lyapunov exponent [panel (b)] on parameter c for $\varepsilon = 0.4$ and $\alpha = 0$, for several values of μ. To reveal that the LE λ is negative (although rather close to zero in some domain) in the whole range of parameters, we show $-\lambda$ in the logarithmic scale in panel (c).
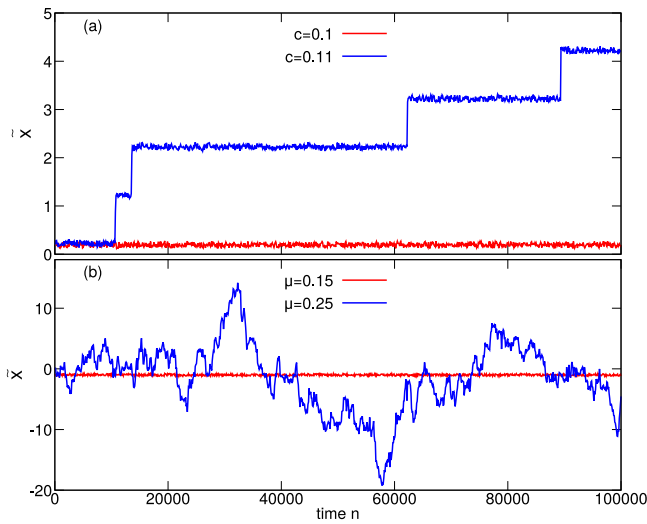
FIG. 3. Time series $\tilde{x}_n$ of the lifted map (1c) with $\varepsilon = 0.4$ and $\alpha = 0$. Panel (a): fixed forcing $\mu = 0.04$ and two values of parameter c, one with zero rotation number, and one where variable $\tilde{x}$ continuously grows. Panel (b): symmetric case $c = 0$. Here for $\mu = 0.15$ there are separated attractor and repeller, and variable $\tilde{x}$ remains bounded. For $\mu = 0.25$, there attractor and repeller have already collided and the evolution of $\tilde{x}$ represents unbounded diffusion.

characterize the attractor). The domain where $\rho = 0$ is that of separated attractor and repeller [like in Fig. 1(a)], because here variations of $\tilde{x}_n$ are bounded. States with $\rho \neq 0$ correspond to the overlapped attractor and repeller [like in Figs. 1(b) and 1(c)]. A separate consideration should be performed at the symmetric case $c = 0$, where the rotation number vanishes due to statistical symmetry $x \leftrightarrow -x$, although the attractor and the repeller can overlap. We illustrate this in Fig. 3, where we show in panel (a) trajectories of $\tilde{x}_n$ in the asymmetric case $c \neq 0$, and in panel (b) in the symmetric case $c = 0$. In the latter situation, an overlap of the attractor and repeller can be detected by following the difference between maximal and minimal values of $\tilde{x}_n$ during a long time interval. As panel (b) of Fig. 3 illustrates, this difference takes large values (definitely larger than one) for overlapping attractor and repeller, and remains small if they do not overlap.

Calculations of the Lyapunov exponent are presented in Fig. 2(b). This quantity remains negative in all cases, the only difference is in the level of the LE: for nearly symmetric overlapping attractor and repeller it is close to zero, while in the non-overlapping case its value is of order one. This property is different from the corresponding feature of an autonomous circle map: there inside Arnold tongues the LE is negative, while it vanishes at the quasiperiodic dynamics outside of the Arnold tongues. For the autonomous Möbius map, which either possesses only one Arnold tongue or otherwise is conjugated to a circle shift (see discussion in the Appendix), the LE vanishes exactly in the whole interval of parameters outside the Arnold tongue. We will further discuss this property of the chaotically driven Möbius map in Sec. IV.

Adopting the criterion for the overlap of the attractor and repeller as described above, we calculate in Fig. 4 an analog of the
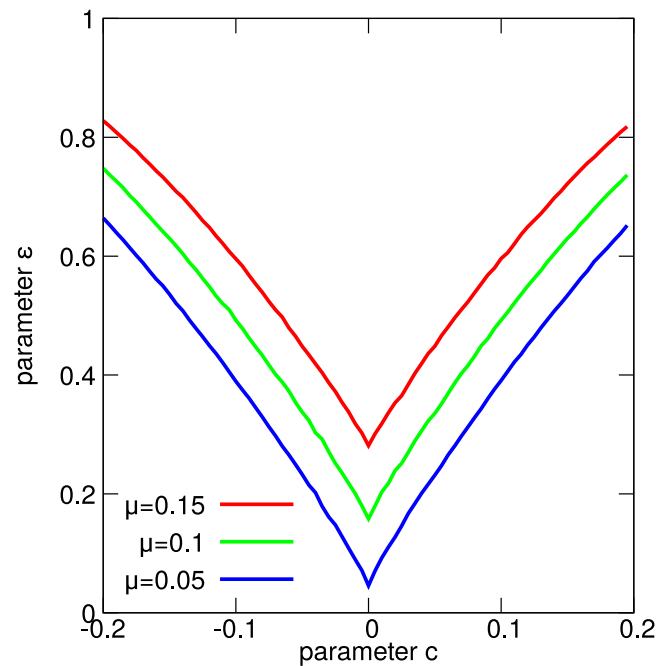

FIG. 4. Domains of existence of attractor and repeller on the (c, ε)-parameter plane (what corresponds to a usual representation of Arnold tongues), for several values of parameter μ and $\alpha = 0$. The attractor and the repeller are separated above the curves, where the rotation number ρ vanishes.

Arnold tongue on the plane of parameters (c, ε) for the system (1). As discussed above, in the context of the phase synchronization theory, these parameters correspond to "frequency mismatch" (parameter c) and the "amplitude of the force" (parameter ε) for a periodically driven chaotic system, internal phase irregularity of which is described by parameter μ. One can see that for large values of parameter μ, larger values of the forcing are needed to "phase synchronize" the system, i.e., to ensure that the attractor and the repeller do not overlap and the rotation number vanishes.

IV. COLLISION OF ATTRACTOR AND REPELLER IN TERMS OF PERIODIC ORBITS

A. Bifurcations of periodic orbits

In descriptions of transitions of chaotic sets, a common approach is to follow the corresponding transitions of saddle periodic orbits, embedded in chaos. In the case of attractor–repeller collision in the skew system (1), this method corresponds to considering bifurcations of the Möbius map (1c), driven by periodic orbits of the Anosov subsystem (1a)–(1b).

These bifurcations are rather simple, because the Möbius map has a special property distinguishing it from generic circle maps: any iteration of a Möbius map is again a Möbius map (although with different parameters, see the Appendix). Thus, for any period-m orbit in the driving (t_n, s_n)-subsystem, the map $x_n \to x_{n+m}$ according to (1) is a Möbius map. Because the latter map is autonomous, it either
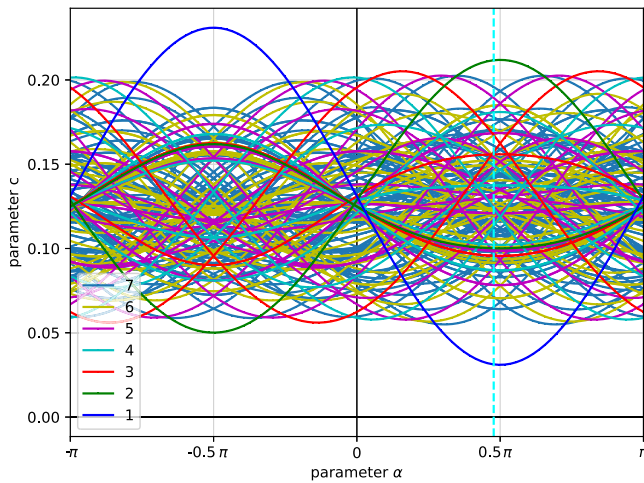
FIG. 5. Curves for saddle-node bifurcations in map (1) for all periodic orbits of the Anosov map with periods up to 7 (curves for the periodic orbits of the same period have the same color, as indexed on the panel), on the plane of parameters (c, ε) for $\varepsilon = 0.4$ and $\mu = 0.1$. The "envelopes" of these curves define border between regimes 1 and 3 (small values of c) and between regimes 2 and 3 (large values of c).

(i) possesses a pair of stable and unstable fixed points (inside the basic "synchronization region," where the rotation number is an integer); (ii) can be transformed by a smooth transformation $x \to y$ to the circle shift $y_{n+m} = y_n + m\rho$, where ρ is the rotation number according to (2) (see the Appendix for details). This number smoothly depends on the parameters so that there are no windows of periodicity (no higher-order Arnold tongues).

This feature of the Möbius map means that for any driving periodic orbit (t_n, s_n), in Eq. (1c) there is just one possible saddle-node (tangent) bifurcation which separates regimes (i) and (ii) above. In Fig. 5, we show these bifurcation curves in the plane of parameters (c, α) for fixed $\varepsilon = 0.4$ and $\mu = 0.1$.

One can see from Fig. 5 that for every value of parameter α there is a range of critical positive values of parameter c, $0 < c_1(\alpha, \mu, \varepsilon) \le c \le c_2(\alpha, \mu, \varepsilon)$, at which different periodic orbits bifurcate (the corresponding interval of negative values of c is $c_3(\alpha, \mu, \varepsilon) \le c \le c_4(\alpha, \mu, \varepsilon) < 0$). We will call these ranges of c *transitional regions*. Thus, the system demonstrates three dynamical states:

1. **Small $|c|$:** Separated attractor and repeller exist for $c_4(\alpha, \mu, \varepsilon) < c < c_1(\alpha, \mu, \varepsilon)$. On these sets the x-coordinates on the attractor and repeller are functions of (t, s). These functions are expected to be relatively smooth for large ε and are non-smooth (fractals) for small ε. All other points of the phase space belong to basins of the attractor (or of the repeller, if one iterates backward in time). The rotation number ρ is zero.

2. **Large $|c|$:** Attractor and repeller overlap and possess no isolated periodic orbits for $c > c_2(\alpha, \varepsilon, \mu)$ and $c < c_3(\alpha, \varepsilon, \mu)$. Thus, there are no hyperbolic sets for this range of parameters. Evolution of variable x for each periodic trajectory of the Anosov map

is described by a superposition of Möbius maps, which results in a Möbius map that is smoothly conjugate to a circle shift. This means that the full system (1) possesses no isolated periodic orbits. The rotation number ρ is non-zero. It is instructive to discuss the Lyapunov exponent in this region. According to calculations shown in Figs. 2(b) and 2(c), it is negative, although small in the absolute value. On the other hand, the LE calculated on any periodic orbit of the Anosov map vanishes (because the Möbius map is conjugated to a circle rotation). Moreover, it is well-known that periodic orbits in the Anosov map are dense. Thus, one cannot obtain the LE for a typical chaotic trajectory in the skew map (1) by virtue of the averaging over values corresponding to periodic orbits. The reason for this paradoxal situation is that the Lyapunov exponent in the x-direction is not an "observable" along a trajectory of the Anosov map, but requires additional averaging over the dynamics of x (and this averaging is not ensured when a chaotic trajectory "jumps" from one periodic orbit to another one).

3. **Moderate $|c|$:** In these transitional regions $c_1 \le c \le c_2$ and $c_3 \le c \le c_4$, some pairs of saddle periodic orbits already disappeared via a saddle-node bifurcation, but some other still exist. Attractor and repeller overlap, but their measures are concentrated in different regions [cf. Fig. 1(b)]. In Sec. V, we construct a heterodimensional cycle in the region $c_1 \le c \le c_2$, i.e., a heteroclinic cycle connecting saddle periodic orbits inherited from the former attractor and the repeller. These periodic orbits have different dimensions of stable and unstable manifolds: those which belong to the attractor have two stable directions (one of them in x variable) and one unstable, and those which belong to the repeller have two unstable directions (one of them in x variable), and one stable. Thus, the dynamics in this region is heterodimensional.

B. First tangent bifurcation

The aim of this section is to show how the attractor and repeller collide at the first tangent bifurcation, and what happens to heteroclinic connections. In region 1 each period-m point P_m^i in the Anosov subsystem (1a)–(1b) corresponds to a pair of period-m orbits A_m^i and R_m^i: A_m^i belongs to the attractor, while R_m^i belongs to the repeller. At the curves $c = c_1(\alpha, \mu, \varepsilon)$ and $c = c_4(\alpha, \mu, \varepsilon)$, one of pairs of these periodic orbits merges via a tangent bifurcation. We illustrate this situation in Fig. 6.

For simplicity, we consider the case where the first tangent bifurcation occurs with fixed points A_1 and R_1. Such a bifurcation occurs as the first one when c increases while parameter α is close to $\alpha = \pi/2$ in Fig. 5(a). Below the curve $c = c_1(\alpha, \mu, \varepsilon)$, all periodic orbits A_m^i of the attractor are intertwined in one homoclinic tangle formed by stable $W^s\left(A_m^i\right)$ and unstable $W^u\left(A_m^i\right)$ invariant manifolds (the same for the repeller). This means that there are heteroclinic connections between all periodic orbits of the attractor (the same for the repeller). Schematically, this is illustrated in Fig. 6(a), where it is shown how the points A_1 and A_2 (and also R_1 and R_2) are connected via a heteroclinic cycle. The points A_1 and R_1 merge at a tangent bifurcation (this is a codimension-one bifurcation of a saddle-saddle fixed point possessing a homoclinic orbit[26]) on the curve $c = c_1(\alpha, \mu, \varepsilon)$, see Fig. 6(b), and disappear above it. One can
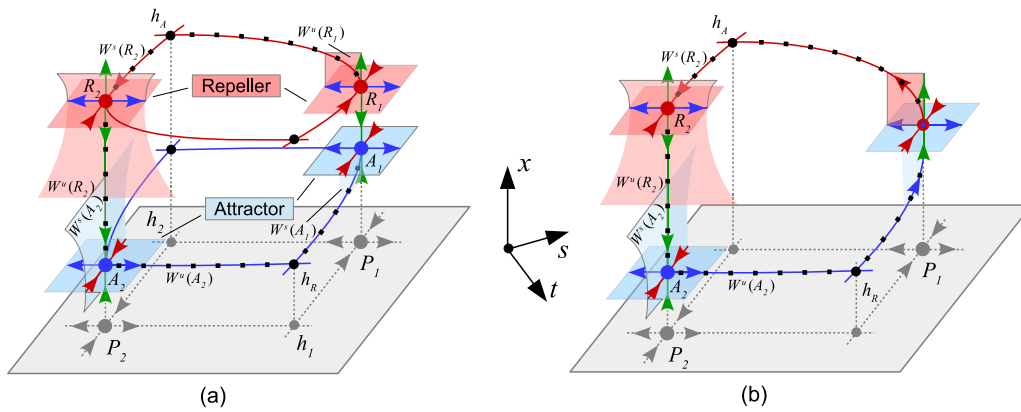
FIG. 6. Illustration of the attractor–repeller collision. (a) Separated chaotic attractor and chaotic repeller at $c_4(\alpha, \mu, \varepsilon) < c < c_1(\alpha, \mu, \varepsilon)$. A_1, A_2 and R_1, R_2 are fixed and period-2 saddle points belonging to the attractor and to the repeller, respectively (we show here every second iteration of the map, thus, both the fixed point and the period-2 point of the original system look like fixed points). (b) On the curves $c = c_1(\alpha, \mu, \varepsilon)$ and $c = c_4(\alpha, \mu, \varepsilon)$ one of pairs of periodic orbits, say A_1 and R_1, merges due to a tangent bifurcation [this situation is depicted in panel (b)], and disappears beyond it. Beyond the first such bifurcation, the attractor and repeller are no longer separated.

see that in region 3, beyond the first tangent bifurcation, trajectories going from the former attractor to the former repeller become possible. We will further explore this in Sec. V.

C. Eyelet intermittency

The transition from regime 1 to regime 3, described in Sec. IV B, often called attractor–repeller collision, has been studied in Refs. 8, 27, 28. The basic observation is that at the initial stage of this transition (i.e., where the regime 3 has just appeared), the rotation number ρ grows very slowly,[8,27,28] namely, as $\log(\rho) \sim -\Delta^{-1/2}$, where Δ is the deviation of parameter c from it critical value (in the situation above $\Delta = c - c_1$). We illustrate this statistical law in Fig. 7, where we show the rotation number in a double logarithmic scale. The reason for such a slow growth of the rotation number lies in the transversal instability of the trajectory connecting former attractor and repeller beyond the first tangent bifurcation at $c = c_1$. Indeed, for a circle map beyond the tangent bifurcation, the characteristic time τ to perform a full rotation scales as $\tau \sim \Delta^{-1/2}$. Thus, in the full system, one can observe such a rotation only if a chaotic trajectory spends at least this time in a small vicinity (say, of size δ) of the saddle periodic orbit in the driving system (1a)–(1b), which is responsible for the tangent bifurcation. Because this periodic orbit is a saddle with the unstable Lyapunov exponent λ^u, an initial point should be in the vicinity of size $\delta e^{-\lambda^u \tau}$ of the periodic orbit in order to remain in this vicinity for time τ. The probability for this is $\sim \delta\, e^{-\lambda^u \tau}$, thus one needs $T \sim \delta^{-1} e^{\lambda^u \tau}$ iterations of the original system to perform one rotation. This yields the estimation of the rotation number $\rho \sim T^{-1} \sim \delta\, e^{-\lambda^u \Delta^{-1/2}}$, from which the expression for the rotation number near the criticality follows (see also Ref. 29 for a similar expression for a circle map with noisy, not chaotic, driving). Although a trajectory connecting attractor and repeller is rather unprobable close to the transition point c_1 in a "free run," such a trajectory can be explicitly constructed, as we will discuss in Sec. V.

We conclude this section with a discussion of validity of the approach to the attractor–repeller collision by virtue of following bifurcations of periodic orbits embedded in chaos. We are not aware of rigorous results proving that indeed such a collision is mediated by the periodic orbit which first undergoes saddle-node bifurcation. However, the diagram shown in Fig. 5 indicates that there are parameter regions where cycles with low periods bifurcate definitely prior to cycles with higher periods. Thus, one hardly expects that a non-periodic orbit can bifurcate prior to the low-periodic cycles. On the other hand, such a case cannot be excluded in general. A search for a situation where a chaotic transition is mediated by a non-periodic orbit appears to be a challenging timely problem in the theory of chaotic transitions.
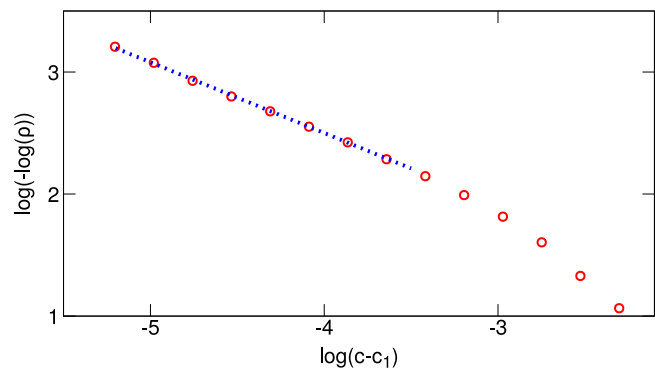

FIG. 7. Dependence of the rotation number on the parameter c close to criticality. Other parameters: $\varepsilon = 0.4$, $\alpha = 1.5$, $\mu = 0.1$, $c_1 = \arcsin(\varepsilon)/\pi - \mu \sin \alpha$. For the calculation of the rotation number, a trajectory of length 5×10^9 was explored. The dotted straight line has a slope -0.58, which slightly deviates from the theoretical prediction 0.5.

V. HETERODIMENSIONAL CYCLES

In this section, we study the intermediate situation (type 3 above) in more detail. Here, the attractor and the repeller overlap (this means that at least one pair of periodic orbits already disappeared via a tangent bifurcation), and this topological object possesses still many saddle periodic orbits from both former attractor and repeller. Let us call them for brevity *A-orbits* and *R-orbits*, respectively. These saddle orbits have different dimensions of stable and unstable manifolds: A-orbits have a two-dimensional stable and one-dimensional unstable manifolds (one stable and one unstable directions from the Anosov map (1a)–(1a), and one stable eigenvector in the x-direction), R-orbits have a one-dimensional stable and two-dimensional unstable manifolds (here, the eigenvector in the x-direction is unstable). This situation is sometimes called *unstable dimension variability* (UDV),[30–32] it has been discussed in mathematical literature[2,4,33–38] and in applications.[39–41]

A characteristic feature of this regime is the existence of heterodimensional cycles[1,6,7] consisting of pairs of heteroclinic trajectories connecting A-orbits with R-orbits: one of these trajectories lies in the transversal intersection of two-dimensional manifolds of A- and R-orbits, while another one passes through a non-transversal (codimension-1) intersection of one-dimensional manifolds of these orbits. The main goal of this section is to provide a numerical evidence for the existence of such cycles in the intermediate case 3. For simplicity, we restrict ourselves to the simplest case where the A- and R-orbits have period two, while the pair of fixed points A_1 and R_1 which used to belong to the attractor and repeller, respectively, already disappeared via a tangent bifurcation (cf. Fig. 6).

In this case, it is more convenient to consider the second iteration of the map. Then, the period-2 points A_2 and R_2 in map (1) becomes fixed points. The corresponding fixed point of the twice-iterated Anosov map (1a)–(1b) is denoted P_2. The fixed point

of the Anosov map is denoted P_1. The cycle that we will construct, starts at A_2. Then, the (t, s)-values become close to the fixed point P_1 and, at these iterations, x-values move from the former attractor to the former repeller through the narrow tunnel [region T in Fig. 8(a)] located on the place where the fixed points A_1 and R_1 existed before the tangent bifurcations. After this, the trajectory comes asymptotically close to R_2. We sketch this trajectory in Fig. 8(a).

For the numerical construction of the cycle described above, we choose the following values of parameters: $\mu = 0.8$, $\varepsilon = 0.4$, $\alpha = 1.5$. Indeed, for these values of the parameter, the Möbius map (1c) at the point P_1 is conjugated to a rotation (i.e., parameters are taken beyond the tangent bifurcation of the corresponding fixed points A_1 and R_1), but the A_2- and R_2-points still exist. In Fig. 5, this situation occurs near $\alpha \approx \pi/2$ above the blue curve corresponding to the tangent bifurcation of the fixed points A_1 and R_1 but below other curves corresponding to the tangent bifurcations of periodic points of higher periods (the adopted parameter value $\alpha = 1.5$ is marked with a dashed cyan line in Fig. 5).

The strategy for this numerical construction consists of two stages. First, we compute a driving one trajectory in the Anosov map (1a)–(1b) as a homoclinic trajectory for the point P_2 which comes very close to the fixed point P_1. At the next stage, we use this trajectory as the driving in the Möbius map (1c) in order to construct the full heteroclinic cycle connecting points A_2 and R_2.

- First, on the (t, s)-plane, we find intersection points h_1 and h_2 of the unstable manifold $W^u(P_2)$ with the stable manifold $W^s(P_1)$, and of the unstable manifold $W^u(P_1)$ with the stable manifold $W^s(P_2)$, respectively, see Fig. 8(b). This is a straightforward task, because all the manifolds are straight lines. Thus, we construct two heteroclinic connections $P_2 \to P_1$ and $P_1 \to P_2$.
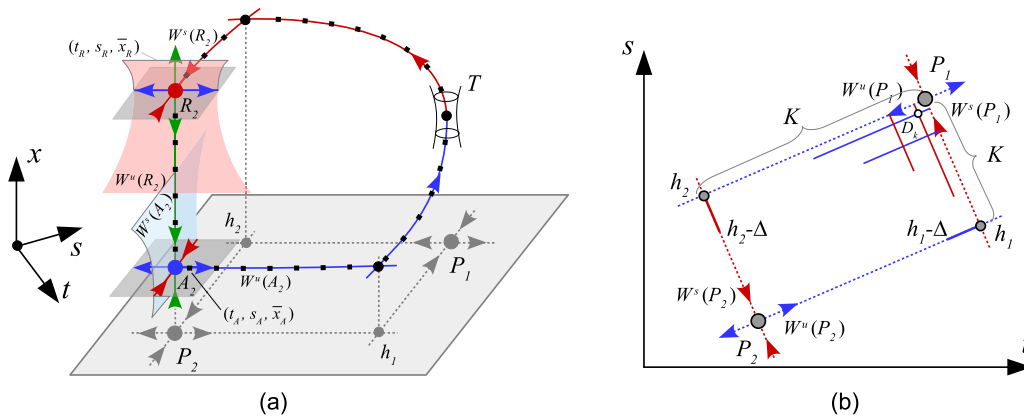

(a)   (b)

FIG. 8. (a) Illustration for the numerical construction of a heterodimensional cycle connecting the points A_2 and R_2. Despite the points A_2 and R_2 this cycle also consists of two orbits (marked by black square dots). One (trivial) orbit belongs to the transversal intersection of two-dimensional manifolds $W^s(A_2)$ and $W^u(R_2)$, along this orbit only variable x varies (so it looks like a vertical line in the figure). Another (nontrivial) orbit passes through the non-transversal (codimension-1) intersection of one-dimensional manifolds $W^u(A_2)$ and $W^s(R_2)$ inside a narrow tunnel T. The points P_1 and P_2 are the fixed and the period-2 points in the Anosov map (1a)–(1b); the heteroclicnic points h_1 and h_2 belong to the intersection $W^u(P_2) \cap W^s(P_1)$ and $W^s(P_2) \cap W^u(P_1)$, respectively. (b) Heteroclinic cycle connecting the points P_1 and P_2. This construction is used to find a homoclinic orbit to the point P_2 in the Anosov map (1a)–(1b). This homoclinic orbit of the Anosov map is then used as a driving trajectory for numerical construction of the heterodimensional cycle.

- Then, we find a homoclinic trajectory of the Anosov map (1a)–(1b) $P_2 \to P_2$ which passes close to the constructed heteroclinic cycles. For this goal, on the unstable manifold $W^u(P_2)$, we take a small segment $[h_1 - \Delta, h_1]$ where the point $h_1 - \Delta$ lies between the points P_2 and h_1. We iterate this segment forward in time (say, we use K iterations), until the iteration of the point h_1 comes sufficiently close to the point P_1. Similarly, on the stable manifold $W^s(P_2)$ we take a small segment $[h_2 - \Delta, h_2]$ where the point $h_2 - \Delta$ lies between the points P_2 and h_2. We iterate it backward in time (again K times) until the iteration of h_2 comes close to the point P_1. This ensures that the corresponding images of the segments $[h_1 - \Delta, h_1]$ and $[h_2 - \Delta, h_2]$ intersect at some point D_k, which is as close to the point P_1 as we want (increasing K we can impose D_k to be arbitrarily close to P_1).

- Iterations of the point D_k in the Anosov map (1a)–(1b) give a homoclinic orbit to the point P_2, which comes very close to the fixed point P_1 and, thus, spends a large time in the vicinity of this point. We will use it as a driving force for the Möbius map (1c).

- In the next step, we find a point (t_A, s_A, x_A) on the unstable manifold $W^u(A_2)$ very close to the point A_2. For this, we take a point (t_A, s_A) which is very close to the point P_2 and, at the same time, belongs to the trajectory of D_k. Then, we select several values x_i close to the x-coordinate of the point A_2, and iterate the points (t_A, s_A, x_i) backward in time. The (t, s)-values converge to the point P_2, while values of x either grow or decrease except for those that belong to $W^u(A_2)$. Taking more x-values between the neighboring points which, by these backward iterations, go along different branches (up and down) of the stable manifold $W^s(A_2)$ in the x-direction, we can find a point (t_A, s_A, x_A) on the unstable manifold $W^u(A_2)$ with desired accuracy. In the same

way, we find a point (x_R, t_R, s_R) lying on the one-dimensional stable manifold of the point R_2.

- Finally, we iterate the points (t_A, s_A, x_A) and (x_R, t_R, s_R), respectively, forward and backward in time until their (t, s)-coordinates reach the point D_k. Generally at this point, the resulting x-coordinates $\bar{x}_A$ and $\bar{x}_R$ do not coincide. However, varying one of the parameters in map (1) (we have varied parameter c), we can find a value at which $\bar{x}_A = \bar{x}_B$. This completes the construction of heteroclinic connection between one dimensional manifolds $W^u(A_2)$ and $W^s(R_2)$ of a particular heterodimensional cycle. The constructed trajectory is illustrated in Fig. 9.

- Note that the intersection of two-dimensional manifolds $W^u(R_2)$ and $W^s(A_2)$ providing the second heteroclinic connection between the points A_1 and A_2 exists always. Thus, the described procedure gives a numerical evidence for the existence of heterodimensional cycles.

In fact, according to the described above procedure, many heterodimensional cycles could be constructed, because there are (infinitely) many different homoclinic orbits to the point P_2, passing close to the point P_1 in the Anosov map. This is, however, not needed, because according to theory developed in Ref. 7, the existence of a (general) heterodimensional cycle implies the existence of many such cycles in a vicinity of parameters values. Our calculations, thus, confirm that at the attractor–repeller collision described by map (1), the heterodimensional dynamics appear. Remarkably, such a regime disappears when the "last" periodic orbits on the attractor and the repeller disappear via a tangent bifurcation (i.e., the system enters regime 2 in the classification of Sec. IV A). This is a particularity of the Möbius map, which has only fixed points but not isolated periodic orbits of higher periods.
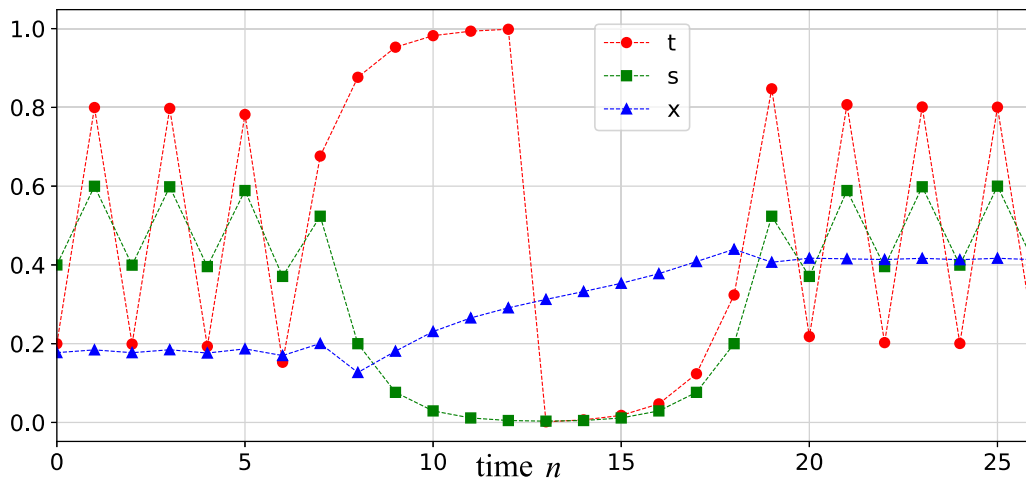

FIG. 9. Illustration of the constructed heteroclinic orbit. Parameters: $\varepsilon = 0.4$, $\alpha = 1.5$, $\mu = 0.08$, $c = 0.071\,124\,956\,712\,020\,02$. One can see that in variables t, s (red and green markers) this trajectory is a homoclinic trajectory to the period-2 cycle (epochs $n < 5$ and $n > 20$), which passes close to the fixed point $t = s = 0$ (epoch $10 \lesssim n \lesssim 15$). During the stay of the (t, s) trajectory close to the fixed point, variable x (blue markers) varies from $x \approx 0.2$ (position of the attractor) to $x \approx 0.4$ (position of the repeller).

VI. VARIABILITY OF THE FINITE-TIME LYAPUNOV EXPONENTS

One of the implications of the heterodimensional dynamics is a strong variability of the Lyapunov exponent. Indeed, consider a situation where the attractor and the repeller overlap and they possess periodic orbits with different stability in the x-direction. Then a trajectory which visits vicinities of these periodic orbits will have positive and negative finite-time Lyapunov exponents, depending on whether this trajectory is close to unstable or to stable in x-direction periodic orbits, respectively. This means that the spread of the finite-time Lyapunov exponents is large and includes positive values, although the average Lyapunov exponent is negative.

To test this property of the heterodimensional dynamics in our system, we calculated finite-time Lyapunov exponents $\lambda_N = \frac{1}{N} \sum_{k=n}^{k=n+N-1} \log \frac{dx_{k+1}}{dx_k}$ for time intervals up to $N = 100$. According to a general scaling of finite-time Lyapunov exponents,[42] the probability to have positive values scales as $P(\lambda_N > 0) \sim \exp[-N\gamma]$ with some positive exponent γ. We illustrate this scaling in Fig. 10 for several values of parameter c. At this point, we would like to justify the chosen range of the time intervals N. According to the theory, one should take N as large as possible for the asymptotic exponential decay of probability above to hold. On the other hand, reliable estimation of very small probabilities is computationally challenging, because it requires very long time series. Figure 10 shows that the chosen range of values of N appears reasonable, because in this full range the dependence of the probability on N appears as exponential with a good precision. Furthermore, we show in the inset the dependence of this exponent on parameter c. One can see that close to the attractor–repeller collision this exponent is large, corresponding to a very small probability to visit the domain of the former repeller. This exponent is small in the domain where the invariant measures of the attractor and the repeller nearly coincide (values of $|c|$ close to 0.5).
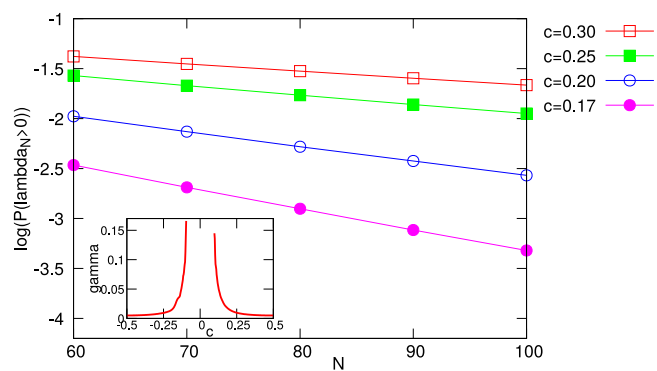
VII. CONCLUSION

The main goal of this paper was to show that robust heterodimensional dynamics naturally appears beyond the attractor–repeller collision in a chaotically driven circle map. We have considered a particular model where the driving system is a hyperbolic Anosov torus map, and the circle map is a Möbius map. Since both subsystems are easily invertible, the attractor and the repeller can simply be followed as the limiting sets of forward and backward iterations, respectively. We traced the collision via tangent bifurcations of the periodic orbits embedded in chaos. Furthermore, we constructed nontrivial heterodimensional cycles inside the overlapped attractor and repeller as trajectories, connecting remaining, not yet bifurcated periodic orbits from the former attractor and repeller. This allows the application of a general theory about the persistence of heterodimensional dynamics.[7] The demonstrated relation of the attractor–repeller collision to the concept of heterodimensional dynamics is the main contribution of this study compared to previous explorations of this transition.[8,27,28]

We also explored properties of the Lyapunov exponent in the driven circle map. This exponent is always negative, which is not surprising for separated attractors and repellers and for a situation close to the attractor–repeller collision. However, we demonstrate that the Lyapunov exponent is also negative, although small in absolute value, in a situation where all periodic orbits in the system have disappeared via a tangent bifurcation. Here, due to peculiar properties of the Möbius map, on every periodic orbit of the driving Anosov map the Lyapunov exponent of the driven map vanishes. Nevertheless, on average the Lyapunov exponent remains negative. Another interesting property of the Lyapunov exponent is that in the case of heterodimensional dynamics, finite-time Lyapunov exponents in the x-direction can be positive. This is because the unstable (in the direction of the circle map) periodic orbits belong to the chaotic set. We confirm that the probability of observing a positive time-N exponent decreases exponentially with N.

AUTHOR DECLARATIONS

Conflict of Interest

The authors have no conflicts to disclose.

Author Contributions

Vladimir Chigarev: Methodology (equal); Software (equal); Validation (equal); Visualization (equal); Writing – review & editing (equal). **Alexey Kazakov:** Conceptualization (equal); Methodology (equal); Validation (equal); Visualization (equal); Writing – original draft (equal); Writing – review & editing (equal). **Arkady Pikovsky:** Conceptualization (equal); Methodology (equal); Visualization (equal); Writing – original draft (equal); Writing – review & editing (equal).

FIG. 10. Illustration of the scaling $P(\lambda_N > 0) \sim \exp[-N\gamma]$ for several values of parameter c for $\varepsilon = 0.4$, $\mu = 0.1$, $\alpha = 1.5$. Markers: calculated probabilities; lines: exponential fit of the data points. The inset shows the exponent γ as a function of parameter c. For small values of c, where the attractor and the repeller are separated, this exponent is not defined because the finite-time exponents are all negative for large enough N.

DATA AVAILABILITY

All numerical experiments with two-dimensional maps are described in the paper and can be reproduced without additional information.

APPENDIX: PROPERTIES OF A MÖBIUS MAP

It is convenient to define a Möbius map as a map of a circle $\psi \to \bar{\psi} = M(\varepsilon, \Phi, \Psi)\psi$, where $0 \leq \psi < 2\pi$,

$$e^{i(\bar{\psi} - \Phi)} = \frac{\varepsilon + e^{i(\psi - \Psi)}}{\varepsilon e^{i(\psi - \Psi)} + 1}. \tag{A1}$$

Using identity $\exp[i\alpha] = \left(1 + i\tan\frac{\alpha}{2}\right)\left(1 - i\tan\frac{\alpha}{2}\right)^{-1}$, we can rewrite the map in a real form as

$$\tan\left(\frac{\bar{\psi} - \Phi}{2}\right) = \frac{1 - \varepsilon}{1 + \varepsilon}\tan\left(\frac{\psi - \Psi}{2}\right). \tag{A2}$$

This form is, however, not convenient for the numerical computation of the rotation number. If we first rewrite (A1) as

$$e^{i(\bar{\psi} - \Phi)} = e^{i(\psi - \Psi)}\frac{1 + \varepsilon\, e^{-i(\psi - \Psi)}}{1 + \varepsilon\, e^{i(\psi - \Psi)}},$$

then another representation

$$\bar{\psi} = \psi + \Phi - \Psi - 2\arctan\frac{\varepsilon\sin(\psi - \Psi)}{1 + \varepsilon\cos(\psi - \Psi)} \tag{A3}$$

follows, which corresponds to Eq. (1c).

For the next calculations, yet another reformulation

$$\bar{\psi} = M(\alpha, z)\psi = e^{i\alpha}\frac{z + e^{i\psi}}{1 + z^* e^{i\psi}} \tag{A4}$$

is suitable, where $z = \varepsilon\exp[i\Psi]$ and $\alpha = \Phi - \Psi$. A direct application of (A4) shows that a composition of two Möbius maps is again a Möbius map,

$$M(\alpha_2, z_2)M(\alpha_1, z_1) = M(\alpha_1 + \alpha_2 + Q, Z),$$
$$Z = \frac{z_1 + \left(z_2\, e^{-i\alpha_1}\right)}{1 + z_1^* \left(z_2\, e^{-i\alpha_1}\right)}, \quad e^{iQ} = \frac{1 + z_1^* \left(z_2\, e^{-i\alpha_1}\right)}{1 + z_1 \left(z_2\, e^{-i\alpha_1}\right)^*}. \tag{A5}$$

Finally, we show that a Möbius map can be transformed (in a certain range of parameters) to a circle shift. The transformation itself is a Möbius transformation with certain complex parameter $s = \kappa\exp[i\xi]$,

$$e^{i\psi} = \frac{s + e^{i\phi}}{1 + s^* e^{i\phi}}. \tag{A6}$$

Substituting this into (A4), one can show that the transformation for ϕ has the form $\bar{\phi} = \phi + \Theta$, provided

$$\kappa = \varepsilon^{-1}\left(\sqrt{\sin^2\frac{\alpha}{2} - \varepsilon^2} - \sin\frac{\alpha}{2}\right), \quad \xi = \frac{\pi}{2} - \frac{\alpha}{2} - \Psi. \tag{A7}$$

One can see that such a transformation is possible if $\varepsilon < \left|\sin\frac{\alpha}{2}\right|$, otherwise the Möbius transformation has a stable and an unstable fixed

points. The rotation number is

$$\Theta = 2\arctan\left(\tan\frac{\alpha}{2}\sqrt{1 - \frac{\varepsilon^2}{\sin^2\frac{\alpha}{2}}}\right). \tag{A8}$$

This conjugation to a circle shift means that the Möbius map has only one Arnold tongue $\varepsilon \geq \left|\sin\frac{\alpha}{2}\right|$, outside of which the rotation number is a smooth function of parameters as follows from relation (A8).

REFERENCES

[1] C. Bonatti and L. J. Díaz, "Persistent nonhyperbolic transitive diffeomorphisms," Ann. Math. **143**, 357–396 (1996).
[2] R. Abraham and S. Smale, "Nongenericity of Ω-stability," Math. Soc., Providence, RI **14**, 5–8 (1970).
[3] L. J. Díaz and J. Rocha, "Nonconnected heterodimensional cycles: Bifurcation and stability," Nonlinearity **5**, 1315 (1992).
[4] L. J. Díaz, "Robust nonhyperbolic dynamics and heterodimensional cycles," Ergod. Theory Dyn. Syst. **15**, 291–315 (1995).
[5] L. J. Díaz, "Persistence of cycles and nonhyperbolic dynamics at heteroclinic bifurcations," Nonlinearity **8**, 693 (1995).
[6] C. Bonatti and L. J. Díaz, "Robust heterodimensional cycles and-generic dynamics," J. Inst. Math. Jussieu **7**, 469–525 (2008).
[7] D. Li and D. Turaev, "Persistence of heterodimensional cycles," arXiv:2105.03739 (2021).
[8] A. Pikovsky, G. V. Osipov, M. Rosenblum, M. Zaks, and J. Kurths, "Attractor–repeller collision and eyelet intermittency at the transition to phase synchronization," Phys. Rev. Lett. **79**, 47–50 (1997).
[9] A. S. Gonchenko, S. V. Gonchenko, A. Kazakov, and D. Turaev, "On the phenomenon of mixed dynamics in Pikovsky–Topaj system of coupled rotators," Physica D **350**, 45–57 (2017).
[10] A. O. Kazakov, "On the appearance of mixed dynamics as a result of collision of strange attractors and repellers in reversible systems," Radiophys. Quantum Electron. **61**, 650–658 (2019).
[11] A. Kazakov, "Merger of a Hénon-like attractor with a Hénon-like repeller in a model of vortex dynamics," Chaos **30**, 011105 (2020).
[12] S. V. Gonchenko, "Reversible mixed dynamics: A concept and examples," Discont. Nonlinearity Complexity **5**, 365–374 (2016).
[13] S. V. Gonchenko and D. Turaev, "On three types of dynamics and the notion of attractor," Proc. Steklov Inst. Math. **297**, 116–137 (2017).
[14] D. Turaev, "A criterion for mixed dynamics in two-dimensional reversible maps," Chaos **31**, 043133 (2021).
[15] A. A. Emelianova and V. I. Nekorkin, "On the intersection of a chaotic attractor and a chaotic repeller in the system of two adaptively coupled phase oscillators," Chaos **29**, 111102 (2019).
[16] G. Ariel and J. Schiff, "Conservative, dissipative and super-diffusive behavior of a particle propelled in a regular flow," Physica D **411**, 132584 (2020).
[17] S. V. Gonchenko, A. S. Gonchenko, and A. O. Kazakov, "Three types of attractors and mixed dynamics of nonholonomic models of rigid body motion," Proc. Steklov Inst. Math. **308**, 125–140 (2020).
[18] S. P. Kuznetsov, V. P. Kruglov, and A. V. Borisov, "Chaplygin sleigh in the quadratic potential field," Europhys. Lett. **132**, 20008 (2020).
[19] A. A. Emelianova and V. I. Nekorkin, "The third type of chaos in a system of two adaptively coupled phase oscillators," Chaos **30**, 051105 (2020).
[20] A. A. Emelianova and V. I. Nekorkin, "Emergence and synchronization of a reversible core in a system of forced adaptively coupled Kuramoto oscillators," Chaos **31**, 033102 (2021).
[21] S. A. Marvel, R. E. Mirollo, and S. H. Strogatz, "Phase oscillators with global sinusoidal coupling evolve by Möbius group action," Chaos **19**, 043104 (2009).
[22] Ch. Gong, R. Toenjes, and A. Pikovsky, "Coupled Möbius maps as a tool to model Kuramoto phase synchronization," Phys. Rev. E **102**, 022206 (2020).

[23]V. Chigarev, A. Kazakov, and A. Pikovsky, "Kantorovich–Rubinstein–Wasserstein distance between overlapping attractor and repeller," Chaos **30**, 073114 (2020).

[24]V. Chigarev, A. Kazakov, and A. Pikovsky, "Mutual singularities of overlapping attractor and repeller," Chaos **31**, 083127 (2021).

[25]Y.-C. Lai and T. Tél, *Transient Chaos* (Springer, New York, 2011).

[26]V. S. Afraimovich and L. P. Shilnikov, "On a bifurcation of codimension 1 leading to the appearance of a countable set of tori," Dokl. Akad. Nauk **262**, 777–780 (1982).

[27]C. Grebogi, E. Ott, and J. A. Yorke, "Fractal basin boundaries, long-lived chaotic transients, and unstable-unstable pair bifurcation," Phys. Rev. Lett. **50**, 935–938 (1983).

[28]C. Grebogi, E. Ott, and J. A. Yorke, "Super-persistent chaotic transients," Ergod. Theory Dyn. Syst. **5**, 341–372 (1985).

[29]G. Olicon Mendez, "Critical behaviour of random diffeomorphisms: Quasi-stationary measures and escape times," Ph.D. thesis (Imperial College London, 2020).

[30]E. J. Kostelich, I. Kan, C. Grebogi, E. Ott, and J. A. Yorke, "Unstable dimension variability: A source of nonhyperbolicity in chaotic systems," Physica D **109**, 81–90 (1997).

[31]S. Das and J. A. Yorke, "Multichaos from quasiperiodicity," SIAM J. Appl. Dyn. Syst. **16**, 2196–2212 (2017).

[32]K. T. Alligood, E. Sander, and J. A. Yorke, "Crossing bifurcations and unstable dimension variability," Phys. Rev. Lett. **96**, 244103 (2006).

[33]D. Li, "Homoclinic bifurcations that give rise to heterodimensional cycles near a saddle-focus equilibrium1," Nonlinearity **30**, 173 (2016).

[34]D. Li and D. Turaev, "Existence of heterodimensional cycles near Shilnikov loops in systems with a $\mathbb{Z}_2$ symmetry," Discrete Contin. Dyn. Syst. **37**, 4399–4437 (2017).

[35]S. Hittmeyer, B. Krauskopf, H. M. Osinga, and K. Shinohara, "Existence of blenders in a Hénon-like family: Geometric insights from invariant manifold computations," Nonlinearity **31**, R239 (2018).

[36]D. Li and D. Turaev, "Persistent heterodimensional cycles in periodic perturbations of Lorenz-like attractors," Nonlinearity **33**, 971 (2020).

[37]S. Hittmeyer, B. Krauskopf, H. M. Osinga, and K. Shinohara, "How to identify a hyperbolic set as a blender," Discrete Contin. Dyn. Syst. **40**, 6815 (2020).

[38]A. Hammerlindl, B. Krauskopf, G. Mason, and H. M. Osinga, "Determining the global manifold structure of a continuous-time heterodimensional cycle," J. Comput. Dyn. **9**, 393–419 (2022).

[39]P. V. Kuptsov, "Violation of hyperbolicity via unstable dimension variability in a chain with local hyperbolic chaotic attractors," J. Phys. A: Math. Theor. **46**, 254016 (2013).

[40]J. C. Vallejo and M. A. F. Sanjuan, "Role of dark matter haloes on the predictability of computed orbits," Astron. Astrophys. **595**, eid A68 (2016).

[41]K. Esashi, T. Onozaki, Y. Saiki, and Y. Sato, "Intermittent transition between synchronization and desynchronization in multi-regional business cycles," Struct. Change Econ. Dyn. **44**, 68–76 (2018).

[42]A. Pikovsky and A. Politi, *Lyapunov Exponents. A Tool to Explore Complex Dynamics* (Cambridge University Press, Cambridge, 2016).